ACS Infectious Diseases

Article

pubs.acs.org/journal/aidcbc

In Vitro and in Vivo Activity of Multitarget Inhibitors against *Trypanosoma brucei*

Gyongseon Yang,[†,‡,#] Wei Zhu,[§,#] Yang Wang,[§] Guozhong Huang,[∥] Soo Young Byun,[†] Gahee Choi,[†] Kai Li,[§] Zhuoli Huang,[⊥] Roberto Docampo,[∥] Eric Oldfield,[*,§] and Joo Hwan No[*,†]

[†]Leishmania Research Laboratory, Institut Pasteur Korea, 696 Sampyeong-dong, Bundang-gu, Seongnam-si, Gyeonggi-do 463-400, Republic of Korea

[‡]Interdisciplinary Programs of Functional Genomics, Yonsei University, Seoul 120-749, Republic of Korea

[§]Department of Chemistry, University of Illinois at Urbana−Champaign, 600 South Mathews Avenue, Urbana, Illinois 61801, United States

[∥]Center for Tropical and Emerging Global Diseases and Department of Cellular Biology, University of Georgia, Athens, Georgia 30602, United States

[⊥]Department of Biochemistry, University of Illinois at Urbana−Champaign, 600 South Mathews Avenue, Urbana, Illinois 61801, United States

Supporting Information

ABSTRACT: We tested a series of amidine and related compounds against *Trypanosoma brucei*. The most active compound was a biphenyldiamidine that had an EC_{50} of 7.7 nM against bloodstream-form parasites. There was little toxicity against two human cell lines with CC_{50} > 100 μM. There was also good in vivo activity in a mouse model of infection with 100% survival at 3 mg/kg i.p. The most potent lead blocked replication of kinetoplast DNA (k-DNA), but not nuclear DNA, in the parasite. Some compounds also inhibited the enzyme farnesyl diphosphate synthase (FPPS), and some were uncouplers of oxidative phosphorylation. We developed a computational model for *T. brucei* cell growth inhibition (R^2 = 0.76) using DNA ΔT_m values for inhibitor binding combined with *T. brucei* FPPS IC_{50} values. Overall, the results suggest that it may be possible to develop multitarget drug leads against *T. brucei* that act by inhibiting both k-DNA replication and isoprenoid biosynthesis.

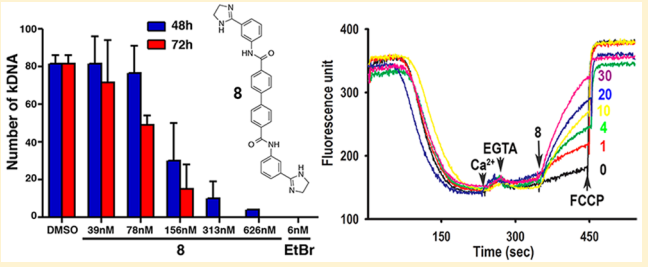

KEYWORDS: *sleeping sickness, kinetoplast DNA, farnesyl diphosphate synthase, proton motive force, computational modeling*

Diseases caused by trypanosomatid parasites afflict millions of individuals worldwide and are the causative agents of sleeping sickness in Africa, Chagas disease in Latin America, and the leishmaniases in India, the Middle East, and Latin America.[1] Many of the drugs used to treat these diseases are quite toxic (arsenicals, antimonials, and benznidazole) or are very expensive or difficult to administer in the field. Plus, many of the drugs that are in use are becoming ineffective because of resistance. Moreover, since there are no vaccines available to prevent these diseases, there is a continuing need for new drugs and new drug leads.

In this work, we focused on sleeping sickness, also known as human African trypanosomiasis (HAT). The disease is transmitted by the bite of the tsetse fly and is fatal if not treated, and resistance to currently used therapeutics is occurring.[2] There are two drugs that are used to treat the initial phase of the disease, suramin (**1**) and pentamidine (**2**) (Figure 1), employed in the treatment of trypanosomiasis caused by *Trypanosoma brucei rhodesiense* and *T. brucei gambiense*, respectively. Pentamidine therapy is rather toxic, and the side effects can be fatal. For the treatment of the second or neurological phase, melarsoprol (**3**), an arsenical, is used for the treatment of both infections. However, this drug likewise causes severe side effects and is lethal in ∼5−10% of patients. Both drugs are taken up into cells by the *T. brucei* adenosine and aquaglyceroporin-2 transporters, and cross-resistance to both drugs is increasing.[2] A newer drug, eflornithine (**4**), alone or in combination with nifurtimox (**5**), has recently been introduced but is effective only for the treatment of *T. brucei gambiense* infections. Other less toxic, inexpensive drugs that are active against infections caused by both species are thus required. There are promising leads that are in clinical trials, such as fexinidazole[3] and oxaboroles,[4] but it is unfortunately true that most clinical trials fail, so there is almost always a need for new concepts and new leads.

Another class of leads are the diamidines. These compounds, such as DB75 (**6**) and its prodrug DB289 (**7**), have been

Received: May 29, 2015
Published: July 19, 2015

DOI: 10.1021/acsinfecdis.5b00068
ACS Infect. Dis. 2015, 1, 388−398

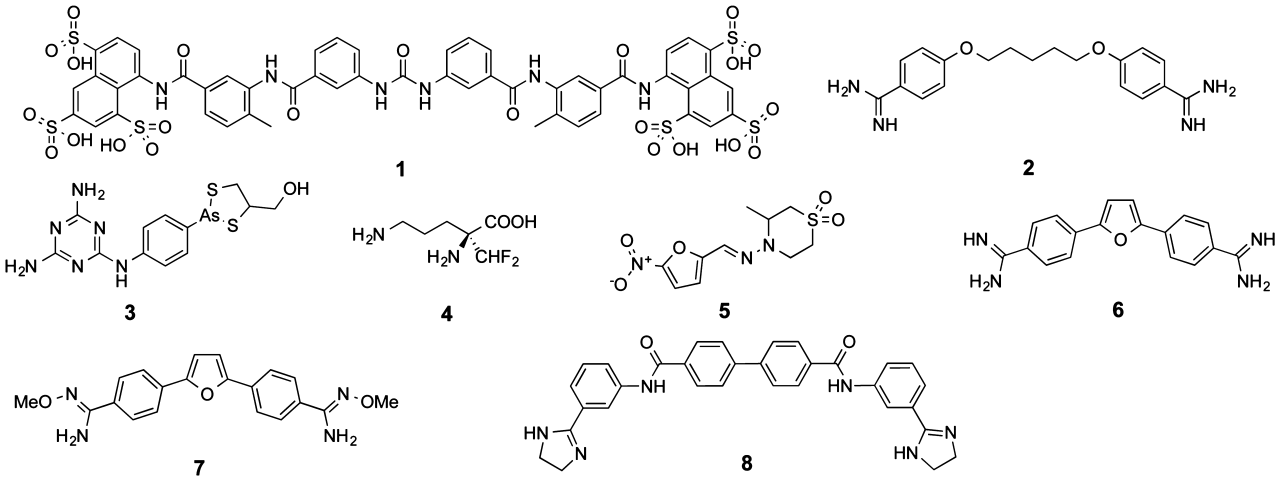

Figure 1. Structures of some *T. brucei* cell growth inhibitors.

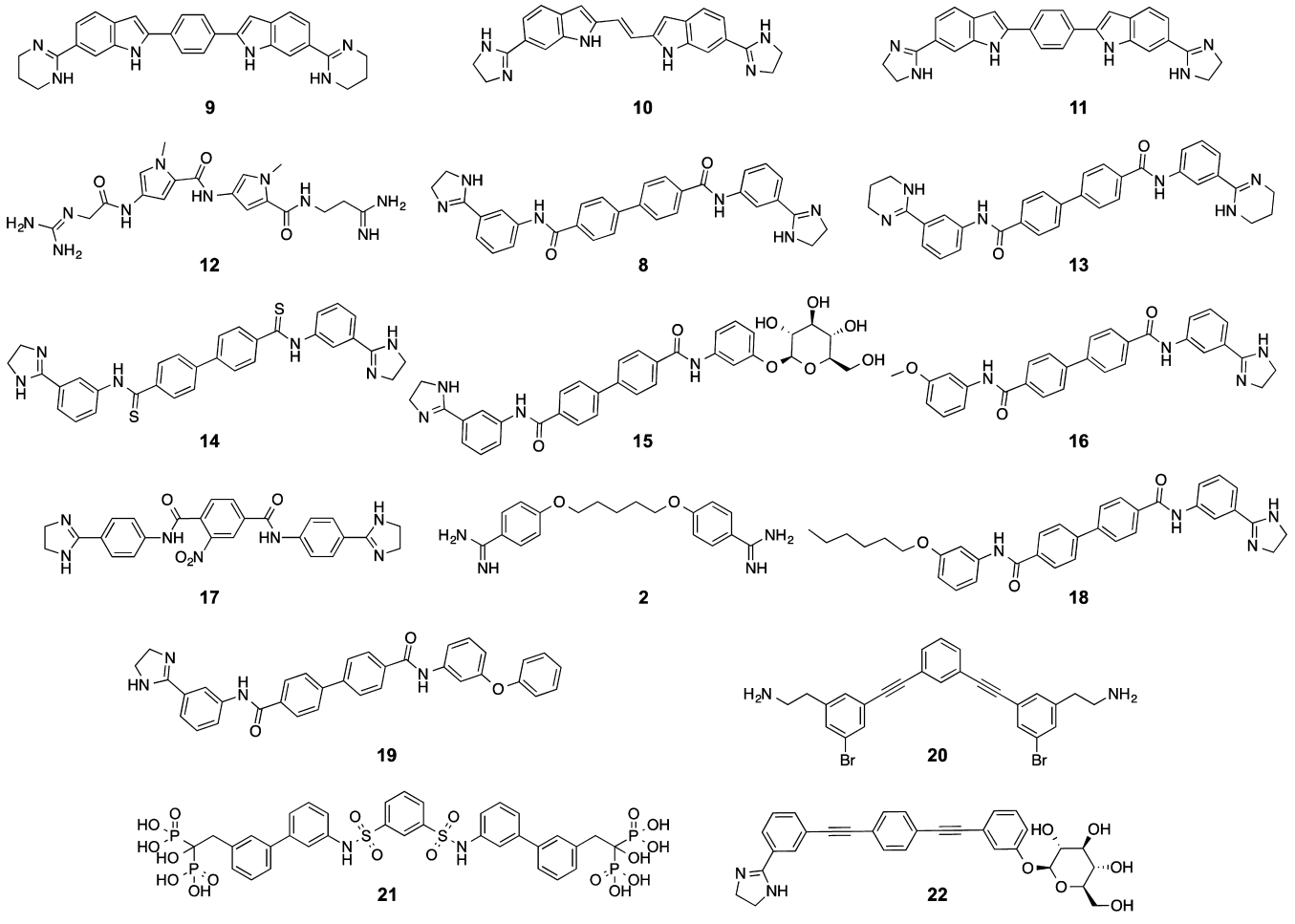

Figure 2. Structures of the 16 compounds investigated here as *T. brucei* cell growth inhibitors.

developed from the diamidine pentamidine and are thought to bind to AT-rich DNA, primarily kinetoplast DNA (k-DNA), but may also have effects as uncouplers,[5,6] compounds that collapse the proton motive force and thus ATP synthesis. Our group recently found that other diamidines, such as BPH-1358 (NSC50460, **8**), exhibit activity against two enzymes involved in isoprenoid biosynthesis, undecaprenyl diphosphate synthase (UPPS)[7] and farnesyl diphosphate synthase (FPPS).[8,9] There was potent (~100 nM) activity against *Staphylococcus aureus* UPPS[7] as well as against *S. aureus* both in vitro and in vivo in a mouse model of infection, with 20 out of 20 mice surviving when treated with **8**[7] while none survived without treatment.[7] In later work,[10] we found that **8** also binds to an AT-rich DNA dodecamer duplex, increasing the unfolding transition (ΔT_m) in a differential scanning calorimetry (DSC) experiment by ~11 °C. We found that we could model *S. aureus* cell growth inhibition quite accurately ($R^2 \approx 0.89$) by using ΔT_m and UPPS IC_{50} results together with one mathematical descriptor,[10]

DOI: 10.1021/acsinfecdis.5b00068
ACS Infect. Dis. 2015, 1, 388−398

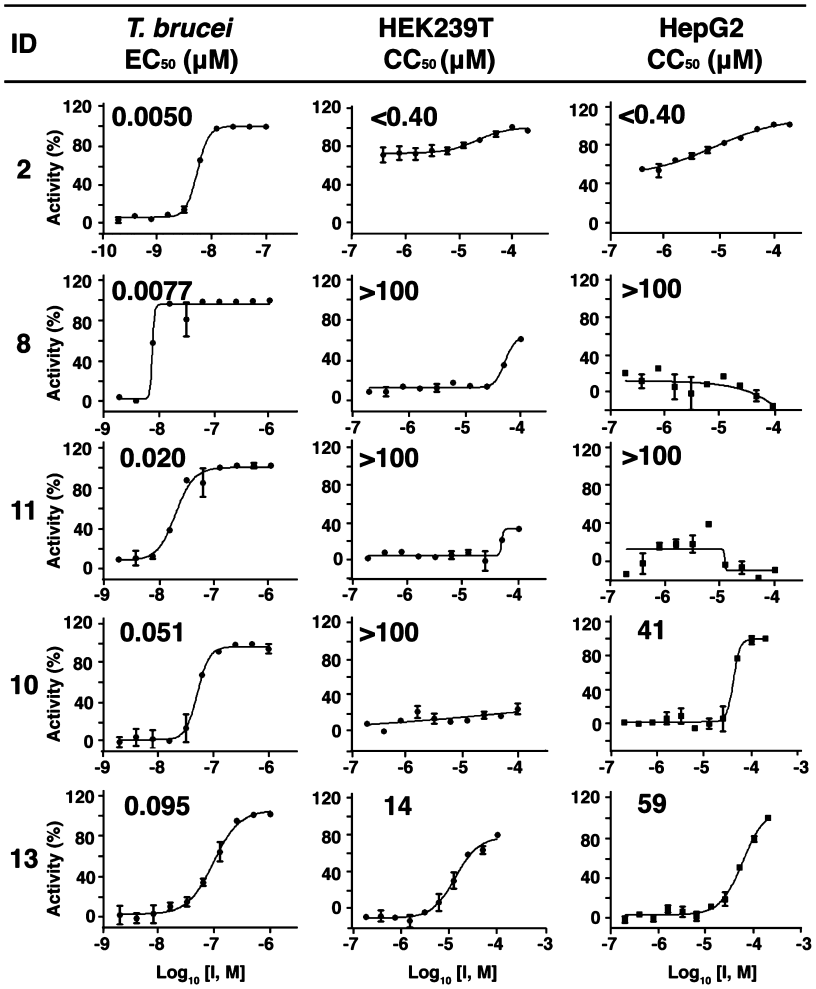

Figure 3. Representative dose−response results for some compounds of interest in *T. brucei*, HEK293T, and HepG2 (human cell) growth inhibition, together with computed selectivity index (SI) values [SI = CC_{50} (human cell line)/EC_{50} (*T. brucei*)]. Experiments were performed in duplicate.

Table 1. Enzyme Inhibition, Cell Growth Inhibition, DSC, and Fluorescence Results

		CC_{50} (μM)[b]		SI[c]				
compd	*T. brucei* EC_{50} (μM)[a]	HEK293T	HepG2	HEK293T	HepG2	ΔT_m (°C)[d]	*F* (A.U.)[e]	*Tb*FPPS IC_{50} (μM)[f]
9	0.084 (0.069−0.1)	>200	>200	>2400	>2400	24	65 ± 5.0	3.5 ± 0.072
10	0.051 (0.041−0.063)	>100	41 (34−50)	>2000	810	20	12 ± 2.6	1.3 ± 0.017
11	0.020 (0.015−0.026)	>100	>100	>5000	>5000	16	25 ± 3.1	9.9 ± 0.50
12	2.1 (1.8−2.4)	>200	>200	>96	>96	16	13 ± 5.8	950 ± 230
8	0.0077 (0.0063−0.012)	>100	>100	>13000	>13000	11	81 ± 2.9	27 ± 0.25
13	0.095 (0.076−0.12)	14 (10−18)	59 (45−77)	140	620	10	140 ± 16	310 ± 93
14	0.85 (0.77−0.93)	27 (21−35)	>100	32	118	7.1	110 ± 16	0.49 ± 0.0088
15	>50	>100	>100	∼2	∼ 2	5.8	19 ± 4.5	21 ± 0.61
16	1.9 (1.4−2.6)	4.7 (4−5.5)	6.4 (5.8−7.2)	2.5	3.4	5.2	55 ± 2.5	18 ± 7.0
17	0.85 (0.62−1.2)	>20	>20	>24	>24	3.9	37 ± 4.4	240 ± 36
2	0.0055 (0.0052−0.0057)	<0.4	<0.4	<80	<80	2.7	64 ± 11	370 ± 7.2
18	0.42 (0.16−1.0)	14 (13−16)	33 (15−73)	35	80	0.7	18 ± 7.7	1800 ± 230
19	0.67 (0.55−0.81)	2 (1.6−2.5)	12 (9.5−15)	3	18	0.6	30 ± 3.3	45 ± 11
20	0.7 (0.66−0.74)	13 (12−15)	6.1 (5−8.7)	19	8.7	0.1	19 ± 8.3	4.4 ± 0.49
21	>50	>100	>100	∼2	∼2	−1.0	7.1 ± 2.4	6.6 ± 2.8
22	23 (5.3−97)	>100	>100	>4.4	>4.4	−1.2	12 ± 2.6	1.9 ± 0.47

[a]Determined from duplicate measurements by nonlinear regression analysis using GraphPad Prism 6. Values in parentheses are 95% confidence intervals. [b]Determined from duplicate measurements. Values in parentheses are 95% confidence intervals. [c]Selectivity index, defined as SI = CC_{50} (HEK293T or HepG2)/EC_{50} (*T. brucei*). [d]Data from ref 10. [e]Fluorescence intensity in arbitrary units. Larger values mean stronger uncoupling effects. Values are reported as mean ± standard deviation (SD) for triplicate experiments. [f]*T. brucei* FPPS IC_{50}. Values are reported as mean ± SD for duplicate experiments.

DOI: 10.1021/acsinfecdis.5b00068
ACS Infect. Dis. 2015, 1, 388−398

implying multitarget inhibition. In the present work, we investigated the activity of each of the compounds reported earlier as *S. aureus* cell growth inhibitors for potential activity against *T. brucei* in vitro, and the most promising compound was tested in vivo. We also tested all of the compounds for activity against *T. brucei* farnesyl diphosphate synthase (*Tb*FPPS), since **8** has been reported to inhibit human FPPS,[8] as well as for activity as uncouplers, since we have found that other lipophilic bases can act as potent uncouplers.[11]

RESULTS AND DISCUSSION

***T. brucei* and Human Cell Growth Inhibition Results.** We first investigated the activity of the 16 compounds whose structures are shown in Figure 2 for activity against *T. brucei* bloodstream-form parasites as well as against two human cell lines, human embryonic kidney (HEK293T) and a human hepatocellular carcinoma (HepG2), as counterscreens for toxicity. The compounds were all from the batches whose synthesis and characterization were reported previously.[10] Representative dose−response results are shown in Figure 3. All of the EC_{50} (for *T. brucei*) and cytotoxicity (CC_{50}) (for HEK293T and HepG2) values obtained are shown in Table 1. As can be seen in Table 1, six compounds (**2**, **8**−**11**, and **13**) exhibited promising activity, with EC_{50} values of <100 nM against *T. brucei* cell growth. The most potent compound was **8**, which had EC_{50} = 7.7 nM, essentially the same as found with **2** (EC_{50} = 5 nM). Perhaps more interesting is the observation that the activity of **8** against both human cell lines was >100 μM, while that of **2** was <0.4 μM. This leads to a "selectivity index" (SI), defined as

$$\mathrm{SI} = \frac{CC_{50}\ (\text{human cell line})}{EC_{50}\ (T.\ brucei)}$$

of >13 000 for **8** versus <80 for **2**, suggesting that **8** might be active in vivo and could have less toxicity than **2**.

Mechanism of Action of Diamidines and Related Compounds. How **8** and the other compounds inhibit *T. brucei* cell growth is of interest since it might eventually lead to more potent and/or selective inhibitors, something that is needed in light of the setbacks found with **7**[12] in clinical trials. All of the compounds described here that exhibit significant activity against *S. aureus* bind to AT-rich DNA,[10] and we previously found that there was a correlation between the number of inhibitor−DNA hydrogen bonds and DNA-binding activity (as determined by ΔT_m, the shift in the maximum of the C_p-versus-T DSC thermogram upon inhibitor binding). Plus, in that earlier work[10] we found that there was a correlation between ΔT_m and *S. aureus* cell growth inhibition. Since binding of diamidines to AT-rich DNA has been implicated in the mechanism of action of other diamidine antibacterials[13] as well as in the inhibition of *T. brucei* cell growth, we sought to determine whether the same mechanism is involved for the compounds described here. As can be seen in Table 1, compounds **8**−**11**, the four compounds with the largest AT-rich DNA ΔT_m values on ligand binding ($\Delta T_m \geq 10$ °C), are all potent *T. brucei* cell growth inhibitors with $EC_{50} \leq$ 100 nM, suggesting a role of DNA binding in *T. brucei* cell growth inhibition. We thus next sought to determine whether **8** (the compound with the best *T. brucei* cell growth inhibition and selectivity index) had any effects on nuclear DNA replication, k-DNA replication, or both. k-DNA, located in the *T. brucei* mitochondria, is an unique form of DNA found only in trypanosomatid parasites and is therefore a good drug target.

Using an EdU click chemistry reaction,[14−16] we found that there was a complete block of *T. brucei* k-DNA replication with **8**, as shown in Figure 4A. EdU is the thymidine analogue 5-ethynyl-2′-deoxyuridine, which when detected using click chemistry with azide-labeled Alexa Fluor 488 leads to green fluorescence in replicating DNA/k-DNA. The diamidine 4′,6-diamidino-2-phenylindole (DAPI) is a highly blue-fluorescent compound when bound to DNA and is used to stain both nuclear and k-DNA. As can be seen in Figure 4A, k-DNA replication in *T. brucei* is completely blocked in the presence of **8**, just as seen with the control, ethidium bromide (bottom panel in Figure 4A). These results show that the diamidine **8** inhibits k-DNA replication, presumably by binding to AT-rich motifs in k-DNA. However, the kinetoplast in *T. brucei* is relatively small compared with that found in another trypanosomatid parasite, *Leishmania donovani*, and as expected, the results of the DAPI (nuclear and k-DNA) staining and the EdU click chemistry (replicating DNA) reactions are much more readily seen with *L. donovani*, as shown in Figure 4B, where clearly, as expected, **8** blocks k-DNA replication. Nevertheless, in both *T. brucei* and *L. donovani*, it appears that **8** inhibits k-DNA replication but has no obvious effect on nuclear DNA replication. These results are consistent with k-DNA replication being one target for **8** in *T. brucei* cell growth inhibition. The actual number of kinetoplasts in the visual field also decreases as a function of drug concentration and incubation time, as shown in Figure 4C for *T. brucei*, indicating kinetoplast disruption.

When we compared the ΔT_m and *T. brucei* cell growth inhibition results (using $pEC_{50} = -\log_{10} EC_{50}$), there was only a poor correlation (R^2 = 0.22; Figure 5A). One possibility for this was that relatively few compounds were investigated (n = 16). Another possibility was that because of the considerable chemical diversity among the 16 structures, good correlations would not be expected since the transport would be very variable. To test this possibility, we added a mathematical descriptor (one of 308 we calculated using the MOE program[17]) and found that the correlation between the predicted and experimental *T. brucei* cell growth inhibition values increased to R^2 = 0.66 with p = 0.001 (Figure 5B). The best mathematical descriptor computed using the MOE program[17] was vsurf_EWmin1. This descriptor, which is the lowest hydrophilic energy (and depends on both the structure connectivity and conformation), gave R^2 = 0.60, p = 0.0004. A third possibility was that multiple targets were involved. This possibility was the one we reported[10] for *S. aureus* cell growth inhibition, in which both DNA binding (major) and UPPS inhibition (minor) were implicated, but there is no UPPS in *T. brucei*. There is, however, another prenyl synthase that is a drug target in *T. brucei*,[18] farnesyl diphosphate synthase, and in earlier work we found that FPPS could be inhibited by diamidines.[8,9]

We thus next screened all 16 compounds against an expressed *T. brucei* FPPS (*Tb*FPPS). All of the enzyme inhibition IC_{50} values are shown in Table 1. The IC_{50} values vary considerably, from ∼490 nM to ∼2 mM. When the *T. brucei* cell growth inhibition (pEC_{50}) results were compared with the *Tb*FPPS inhibition results, there was essentially no correlation (Figure 5C), but the correlation improved to R^2 = 0.71 with the addition of one computed descriptor (PEOE_VSA_FPPOS, the fractional positive polar van der

DOI: 10.1021/acsinfecdis.5b00068
ACS Infect. Dis. 2015, 1, 388−398

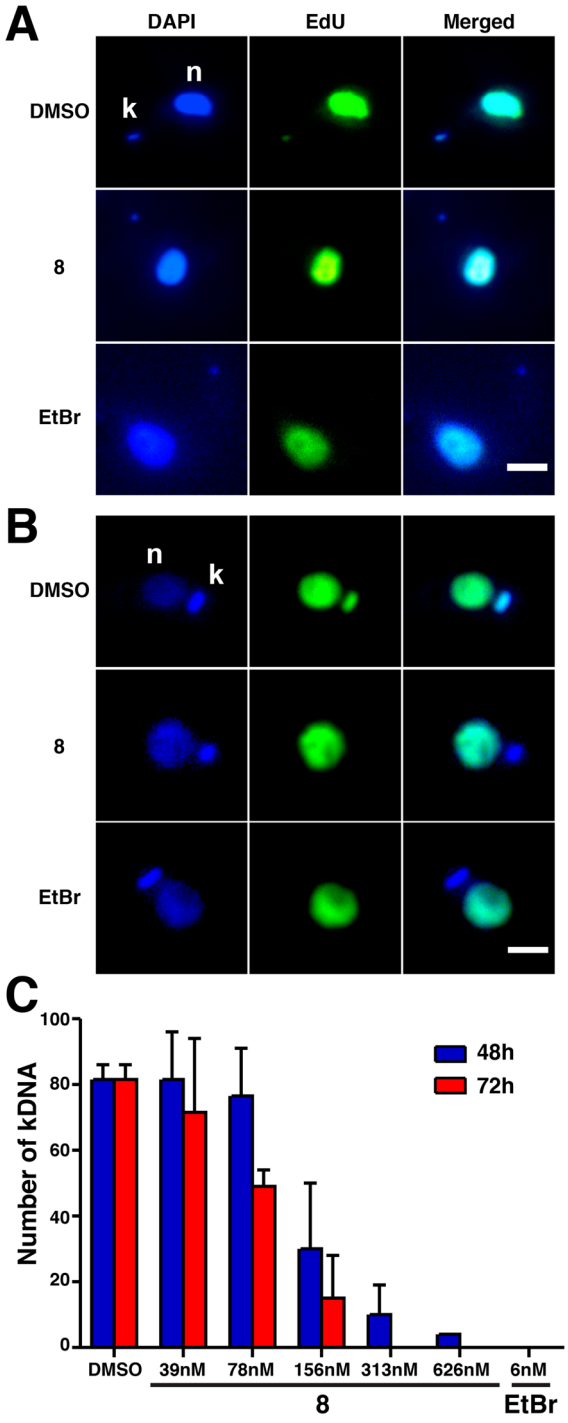

Figure 4. Effects of **8** on nuclear DNA and k-DNA replication for (A, C) *T. brucei* and (B) *L. donovani*. Shown in the top row in (A) and (B) are control (DMSO vehicle) results with DAPI and EdU. DAPI stains all DNA, and the bound compound exhibits blue fluorescence. EdU is used to detect replicating DNA and fluoresces green. In the DMSO controls, both nuclear (n) and k-DNA (k) replicate in both organisms (green). In the middle row in (A) and (B), cells were treated with **8**, which blocks k-DNA replication, so the replicating kinetoplast k-DNA (green) signal is not observed. The same inhibition of k-DNA replication was found with the DNA intercalator ethidium bromide, shown in the bottom row in (A) and (B). Scale bars are 2 μm. Shown in (C) is the number of kinetoplasts in the visual field as a function of **8** concentration (from 39 to 626 nM) and incubation time (48 or 72 h). Values are reported as mean ± SD for duplicate experiments.

Waals surface area, computed using the MOE program[17]) (Figure 5D). When we used both ΔT_m and FPPS data to predict activity,

$$pEC_{50}(\text{cell, predicted}) = a \cdot pIC_{50}(Tb\text{FPPS}) + b\Delta T_m + c$$

the correlation was again poor (R^2 = 0.28; Figure 5E), but it improved to R^2 = 0.76 with p = 0.0005 upon the addition of one computed descriptor, as shown in Figure 5F. These results support the idea that both k-DNA binding and FPPS inhibition may contribute to *T. brucei* cell growth inhibition. To put these R^2 values in perspective, in earlier work[19] we compared 10 sets of enzyme inhibition/cell assay results for diverse systems (antibacterial, antiprotozoal, anticancer, antiviral) and found that on average the enzyme/cell pIC_{50}/pEC_{50} correlations were remarkably poor ($R^2 \approx 0.30$),[19] even though in most cases highly homologous series of compounds were being investigated. The correlation greatly improved when mathematical descriptors (such as clogP) were added, and on average the R^2 values increased to 0.70 (with two added descriptors and large data sets). The same general approach can be used with multiple experimental descriptors, and with *S. aureus* we found R^2 = 0.75 using ΔT_m and UPPS inhibition data, which improved to R^2 = 0.89 with one computed descriptor.[10] It is possible that there are alternate targets whose inhibition is reflected in the computational descriptors, although the use of the experimental ΔT_m and *Tb*FPPS pIC_{50} values together with just one computed descriptor does give a very good prediction of the activity (R^2 = 0.76, p = 0.0005). Interestingly, we also found that the IC_{50} of DB75 (**6**) was ~50 μM against both human and *T. brucei* FPPS. This seems to be a rather large value, but FPPS could be a target for this compound in *T. brucei* since it is likely to be taken up by transporters and could accumulate within the cells, contributing to the toxicity seen with the prodrug DB289.[20]

In addition to k-DNA and FPPS as potential targets, there are of course other possibilities, as suggested by the literature. Specifically, it has been found that pentamidine (**2**) is an uncoupler of oxidative phosphorylation in isolated rat liver mitochondria[21] and that the mitochondria in *T. brucei* are the target of the trypanocidal action of the diamidine DB75.[22] We thus next tested the most promising lead **8** for its ability to collapse the proton motive force (PMF) (here, primarily the mitochondrial membrane potential, $\Delta\psi_m$) in digitonin-permeabilized *T. brucei* bloodstream-form (BSF) trypanosomes (Figure 6A) and procyclic-form (PCF) trypanosomes (Figure 6B–D) using the safranine method.[23,24] We chose compound **8** since it had no effect on the growth of either of the two human cell lines (CC_{50} > 100 μM) but was the most potent *T. brucei* cell growth inhibitor, and as we show below, it is active in vivo.

Figure 6A shows that addition of 10 μM **8** decreased $\Delta\psi_m$, which was further reduced by addition of 8 μM carbonyl cyanide 4-(trifluoromethoxy)phenylhydrazone (FCCP) (2 μg/mL), a potent protonophore uncoupler. Similar results were obtained with PCF trypanosomes (Figure 6B). *T. brucei* PCF mitochondria were able to phosphorylate ADP, as demonstrated by the small decrease in $\Delta\psi_m$ after its addition (Figure 6C). This activity was inhibited by the ATP synthase inhibitor oligomycin. In addition, the mitochondria were able to transport Ca^{2+}, as shown by the decrease in $\Delta\psi_m$ after addition of $CaCl_2$, and the $\Delta\psi_m$ returned to basal levels after addition of the Ca^{2+} chelator EGTA (Figure 6C). Further addition of **8** followed by FCCP again collapsed $\Delta\psi_m$ (Figure 6C). **8** collapsed $\Delta\psi_m$ in a dose-dependent manner (Figure 6D), and **8**

DOI: 10.1021/acsinfecdis.5b00068
ACS Infect. Dis. 2015, 1, 388–398

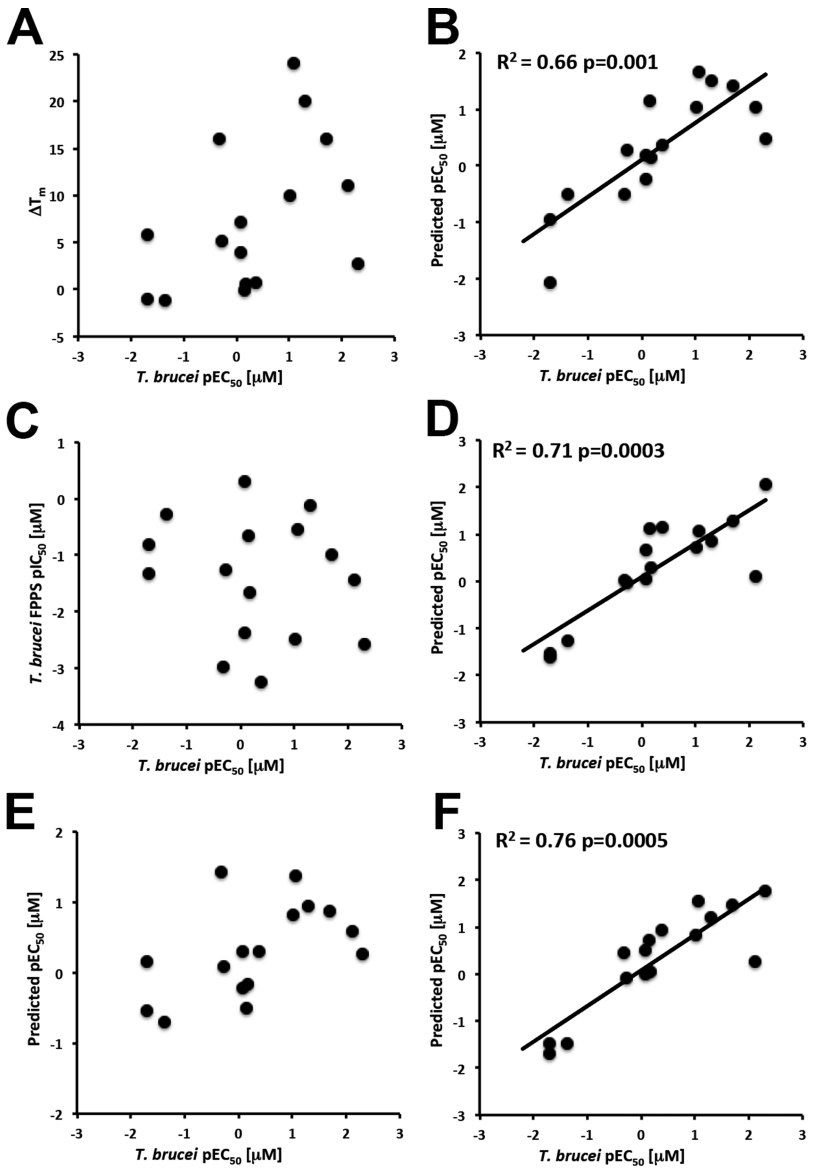

Figure 5. Plots of experimental properties and computed growth inhibition models versus experimental *T. brucei* cell growth inhibition (expressed as pEC_{50}): (A) ΔT_m, $R^2 = 0.22$, $p = 0.07$; (B) ΔT_m + vsurf_EWmin1, $R^2 = 0.66$, $p = 0.001$; (C) FPPS pIC_{50}, $R^2 = 0.03$, $p = 0.53$; (D) FPPS pIC_{50} + PEOE_VSA_FPPOS, $R^2 = 0.71$, $p = 0.0003$; (E) FPPS pIC_{50} + ΔT_m, $R^2 = 0.28$, $p = 0.12$; (F) FPPS pIC_{50} + ΔT_m + PEOE_VSA_FPPOS, $R^2 = 0.76$, $p = 0.0005$.

alone had no effect (Figure 6B). Figure S1 presents the results of three independent experiments. These results show that mitochondria in permeabilized *T. brucei* are able to develop a $\Delta\psi_m$, phosphorylate ATP, and transport Ca^{2+} and that **8** collapses $\Delta\psi_m$. These effects on the PMF are rapid, are very similar to those observed for SQ109 in bacterial systems,[11] and are likely to make a contribution to inhibition of cell growth by **8**.

These observations then raise the following question: do some of the other compounds affect the PMF? We thus next measured the collapse in $\Delta\psi_m$ for all of the compounds, but this time at just a single inhibitor concentration (5 μM). The results are shown in Figure 7. As a control, we used FCCP. The three most potent uncouplers among the compounds shown in Figure 2 were **13**, **14**, and **8** (Figure 7). All of these are biphenyls, with the six-membered amidine **13** being the most effective species, albeit less so than FCCP (140 vs 230 (arbitrary) fluorescence units, respectively). The six-membered ring species **13** was more effective than **8**, which has five-membered amidine rings. The next most active species were **2** and **9**. However, we did not obtain improved growth inhibition models using the uncoupling results, although they may be important for individual compounds.

In addition to the effects on $\Delta\psi_m$, we found that there are deranged mitochondrial morphologies exhibited by *T. brucei* BSF trypanosomes upon treatment with **8**. Figure 8 shows DMSO control cells and cells treated with 500 nM **8** for 24 h. DAPI (blue fluorescence) stains the nuclear DNA and k-DNA, while MitoTracker Red (red fluorescence) is used to visualize the mitochondria, and its uptake depends on $\Delta\psi_m$. As can be seen in Figure 8, k-DNA is localized to the mitochondrion, but the mitochondrial morphology is disrupted by **8**, changing from a normal tubular shape to a more condensed form, particularly toward the location near the k-DNA.

These uncoupling effects are clearly interesting, but they could lead to toxicity, as might human FPPS inhibition.

DOI: 10.1021/acsinfecdis.5b00068
ACS Infect. Dis. 2015, 1, 388−398

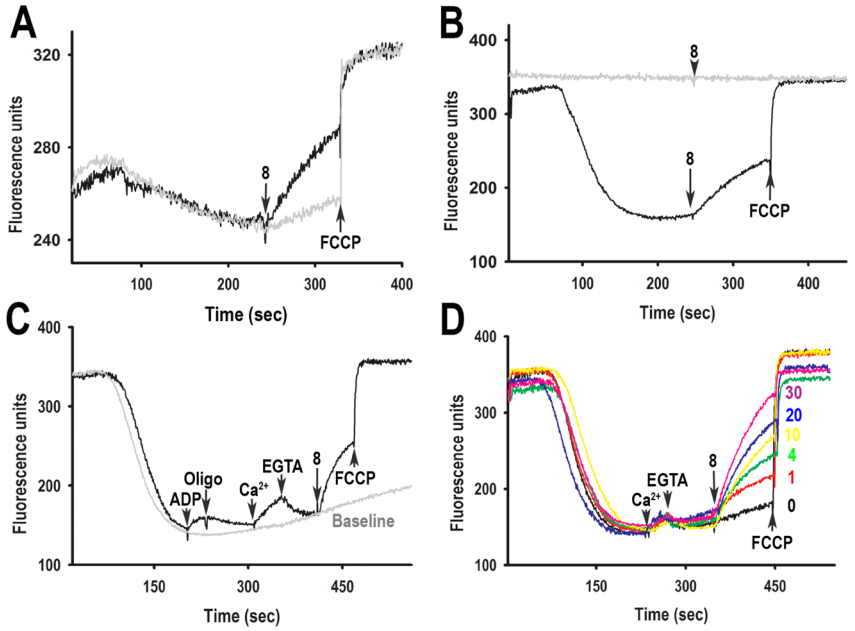

Figure 6. Effects of **8** on the mitochondrial membrane potential $\Delta\psi_m$ in digitonin-permeabilized *T. brucei*. (A) BSF trypanosomes (2×10^8 cells) were added to buffer (2 mL) containing 20 μM EGTA, 1 mM ATP, 500 μM sodium orthovanadate, and 5 μM safranine, and the reaction was initiated with 40 μM digitonin. **8** and FCCP were added where indicated. The gray line is the baseline. (B) PCF trypanosomes (5×10^7 cells) were added to buffer (2.4 mL) containing 2 mM succinate and 5 μM safranine, and the reaction was initiated with (black trace) or without (gray trace) 50 μM digitonin. **8** (5 μM) and FCCP (8 μM) were added where indicated. (C) as in (B) but ADP (10 μM), oligomycin (Oligo) (2 μg/mL), $CaCl_2$ (12 μM), EGTA (200 μM), **8** (10 μM), and FCCP (8 μM) were added where indicated. (D) as in (B), but $CaCl_2$ (12 μM), EGTA (200 μM), various concentrations of **8** (0–30 μM), and FCCP (8 μM) were added where indicated.

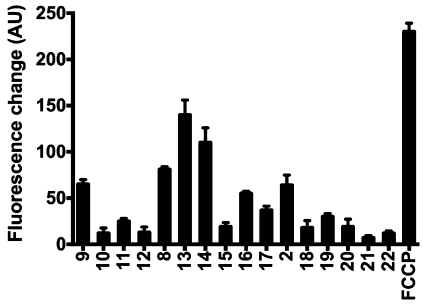

Figure 7. Effects of compounds on the mitochondrial membrane potential $\Delta\psi_m$ in digitonin-permeabilized *T. brucei* PCF trypanosomes. PCF trypanosomes (5×10^7 cells) were added to reaction buffer (1.95 mL) with additions as described in Figure 6B. The chart shows the change in safranine fluorescence (AU = arbitrary units) after addition of each compound (5 μM) or FCCP (5 μM). The results are shown as mean ± SD of three independent experiments.

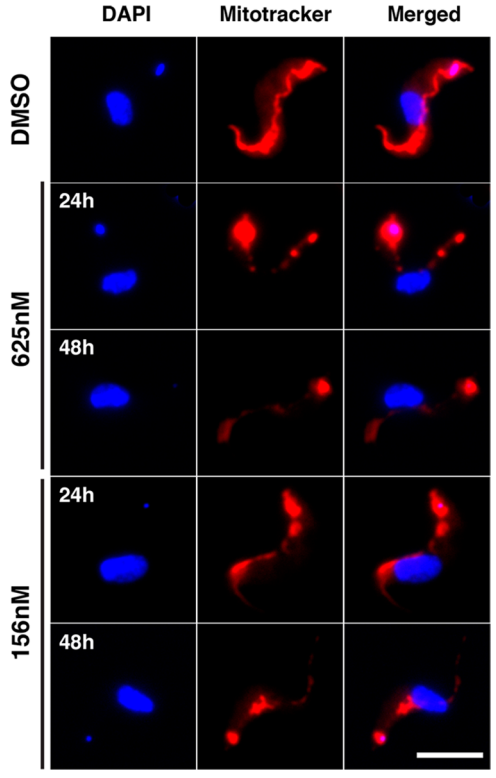

Figure 8. Effects of **8** (156 and 625 nM, 24 and 48 h) on *T. brucei* cells. DAPI fluoresces blue and stains DNA; Mitotracker Red fluoresces red and is used to locate the mitochondrion. The scale bar is 5 μm.

However, in other work[11] we reported that the tuberculosis (TB) drug lead SQ109 acted at least in part as an uncoupler, and this work has now been extended[25] to numerous other TB drug leads, including adamantylureas, indolecarboxamides, tetrahydropyrazolopyrimidines, and the 1,5-diarylpyrrole BM212,[25] all of which are now thought to function primarily as uncouplers. Moreover, drugs such as niclosamide function in the same way[26] and are of interest as diabetes drug leads.[27,28] We thus next sought to determine whether **8** has any efficacy in vivo and/or is highly toxic.

In Vivo Activity in a Mouse Model of Infection. Compound **8** has the best computed SI in both cell lines and also has essentially the same activity as pentamidine (**2**), so it was chosen for further investigation. We used the *T. brucei brucei* Lister 427 mouse model of infection, in which all mice die ~6 days after infection in the absence of any treatment. In an initial set of experiments, mice were treated with PBS, **2** at 5

DOI: 10.1021/acsinfecdis.5b00068
ACS Infect. Dis. 2015, 1, 388–398

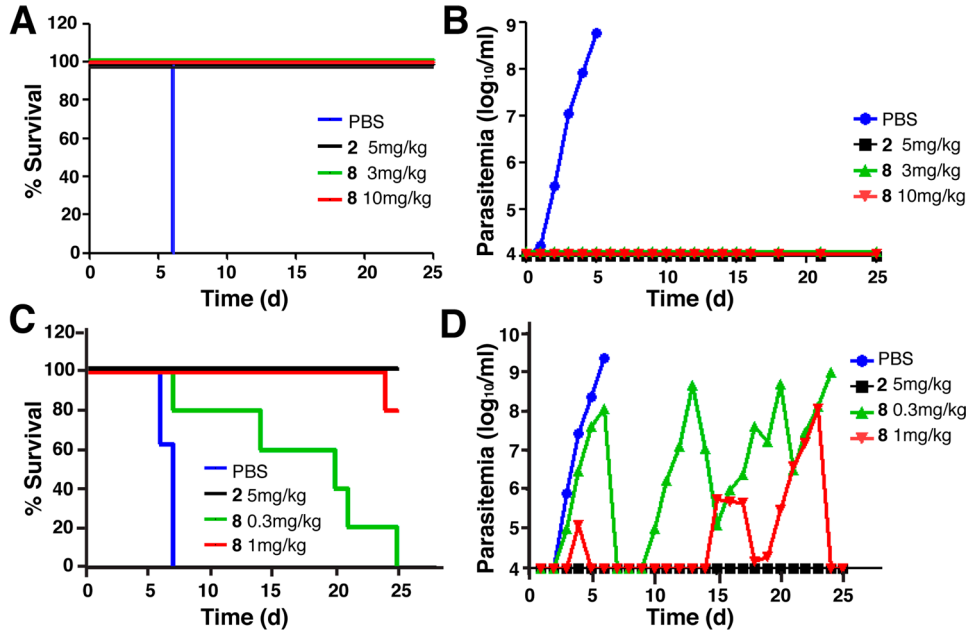

Figure 9. In vivo results for the *T. brucei brucei* Lister 427 mouse model of infection. (A) Mouse survival after treatment with **8** at 3 and 10 mg/kg i.p. for 4 days. (B) Parasitemia as a function of time after treatment. (C, D) Same as (A, B) but at 0.3 and 1 mg/kg i.p.

mg/kg i.p., or **8** at 3 or 10 mg/kg i.p. for 4 days, and Figure 9A shows the survival as a function of time. All of the mice treated with **8** survived in this infection model at both 3 and 10 mg/kg after the 4 day treatment (and over the 25 day observational period), and no parasitemia was observed in the mice treated with **2** or **8** (Figure 9B). We then carried out a second series of experiments, this time at 1 and 0.3 mg/kg i.p. for 4 days. Survival and parasitemia results are shown in Figures 9C, D and indicate (when compared with the results in Figures 9A, B) that the lowest effective dose is ~3 mg/kg. There is no weight loss during mice treatment.

Conclusions. The results presented here suggest that it may be possible to develop new multitarget inhibitors of *T. brucei* cell growth that target both parasite-specific kinetoplast DNA (k-DNA) and isoprenoid biosynthesis (FPPS), with such "multitarget" inhibition being of general interest since it could lead to more effective and more "resistance-resistant" drugs.[29] Of particular interest is the observation that the lead **8** inhibits k-DNA replication but not nuclear DNA replication. Some of the diamidine analogues also inhibited the isoprenoid biosynthesis enzyme farnesyl diphosphate synthase. This is of interest since FPPS is an essential protein for *T. brucei* cell growth.[18] Plus, other compounds acted as uncouplers, which is of interest since other new drug leads against bacteria have been reported to act in this way. In a mouse model of infection, all mice survived upon treatment with **8**, and a similar result with **8** has been reported with *S. aureus* infection in which both DNA and another isoprenoid biosynthesis enzyme, UPPS, were targeted.[7,10] **8** also acts as an uncoupler in both bloodstream-form and procyclic-form parasites, rapidly collapsing the mitochondrial membrane potential $\Delta\psi_m$. However, while **8** was a potent inhibitor of *T. brucei* cell growth, it was a poor inhibitor of the growth of two human cell lines and did not appear to be toxic in mice. The basic observation that k-DNA, FPPS, and the proton motive force can be targeted is thus of general interest in the context of developing new antiparasitic drug leads for treating infections caused by trypanosomatid parasites.

METHODS

Ethics Statement. All animal care and therapy studies were carried out in strict accordance with the guidelines and principles established by the Korean Animal Protection Law (http://animalrightskorea.org). Animal use protocol no. IPK-13009-1 was reviewed and approved by the Institutional Animal Care and Use Committee (IACUC) of the Institut Pasteur Korea.

Inhibitors. Inhibitors were from batches whose synthesis (or availability) and characterization were described previously.[10] All of the compounds were ≥95% pure as determined by elemental analysis or analytical HPLC/MS analysis and were also characterized by ^{1}H NMR spectroscopy and high-resolution mass spectrometry.

Parasites and Cell Culture. *T. brucei brucei* Lister 427 (bloodstream form) was cultivated at 37 °C with a 5% CO_2 atmosphere in HMI-9 medium supplemented with 10% fetal bovine serum (FBS). *T. brucei* was subcultured every 3 or 4 days and maintained until the 20th passage. The HEK239T and HepG2 cell lines used in the cytotoxicity testing were cultivated at 37 °C in a 5% CO_2 atmosphere in Dulbecco's modified Eagle's medium supplemented with 10% FBS.

***T. brucei* Growth Inhibition.** *T. brucei* cell growth inhibition was assayed by measuring the conversion of resazurin to resorufin. Assays were performed in duplicate in 384-well plates that were seeded with *T. brucei* (2.5×10^3 cells per well). After the parasites were seeded, they were exposed to the compounds for 3 days. Resazurin sodium salt (120 μM; R7017; Sigma-Aldrich, St. Louis, MO, USA) was then added, and the plates were incubated for 5 h. After incubation, the parasites were fixed with 4% paraformaldehyde, and the plates were analyzed in a Victor 3 plate reader (PerkinElmer, Waltham, MA, USA) with excitation at 530 nm and emission at 590 nm. Pentamidine was used as a reference drug in the *T. brucei* inhibition assay. The EC_{100} of pentamidine was taken as the concentration that produced 100% growth inhibition.

DOI: 10.1021/acsinfecdis.5b00068
ACS Infect. Dis. 2015, 1, 388−398

Cytotoxicity Assay. A resazurin cytotoxicity assay was performed in duplicate with HEK239T and HepG2 cell lines. Cells (4.0×10^3 cells per well) were seeded in 384-well plates and incubated for 72 h with selected compounds. Cells were then exposed to 40 μM resazurin for 5 h to allow for conversion to resorufin by aerobic respiration. After incubation, cells were fixed with 4% paraformaldehyde, and the plates were read with a Victor 3 plate reader (PerkinElmer) with excitation at 530 nm and emission at 590 nm. Chlorpromazine was used as a reference drug in the cytotoxicity assay. The EC_{100} of chlorpromazine was taken as the concentration that produced 100% growth inhibition.

Protein Expression and Purification. *Tb*FPPS was cloned and expressed as reported previously.[30] Briefly, DNA coding for *Tb*FPPS was cloned into the pET-28a vector (Novagen, Madison, WI, USA). The recombinant plasmid was transformed into an *Escherichia coli* BL21 (DE3) host to be expressed. Bacterial clones were grown in LB medium to an optical density at 600 nm of 0.8 and were induced with 1 mM isopropyl β-D-1-thiogalactopyranoside (IPTG) at 37 °C. After induction for 5 h, the cells were resuspended in binding buffer (500 mM NaCl, 20 mM Na_2HPO_4, pH 7.4) and incubated with 10 mg/mL lysozyme, 10 μg/mL protease inhibitor, and 1 μL/mL benzonase nuclease (Novagen) for 15 min on ice. The supernatant was obtained by centrifugation at 15000*g* for 1 h at 4 °C. Lysates were applied to a nickel-chelated agarose affinity column and washed with binding buffer. Protein was eluted from the column using binding buffer containing 500 mM imidazole. The eluted fraction was desalted with a PD-10 desalting column (GE Life Sciences, Pittsburgh, PA, USA) and stored in 10 mM HEPES buffer (pH 7.4) containing 10 mM 2-mercaptoethanol.

In Vitro Enzyme Assay. *Tb*FPPS inhibition assays were carried out as described previously.[30] Briefly, the condensation of geranyl diphosphate (GPP) with isopentenyl diphosphate (IPP) catalyzed by FPPS was monitored using a coupled colorimetric assay[31] in 96-well plates with 200 μL reaction mixtures containing 400 μM methylthioadenosine (MESG), 100 μM IPP, and 100 μM GPP in 25 mM Tris-HCl (pH 7.4), 1 mM $MgCl_2$, and 0.01% Triton X-100. The highest concentration of the inhibitors in the assay was 316 μM.

Visualization of DNA Replication. After treatment with inhibitors for 72 h, *T. brucei* BSF trypanosomes were incubated for 16 h with the thymidine analogue EdU. EdU-labeled parasites were then washed with 1× PBS, fixed in 100% cold ethanol, and completely dried. Fixed parasites were washed with 1× PBS and incubated with Alexa Fluor 488 azide (Invitrogen, Grand Island, NY, USA) under Cu(I)-catalyzed click reaction conditions (100 μM ascorbic acid and 1 μM $CuSO_4$). EdU-labeled parasites were counterstained with 10 μg/mL DAPI and then mounted in VECTASHIELD mounting medium (Vector Laboratories, Burlingame, CA, USA). The images were analyzed using a Nikon Eclipse 90i fluorescence microscope (Nikon, Tokyo, Japan) and captured with a digital camera (DS-1QM, Nikon).

Visualization of Mitochondrial Membrane Potential. After compound treatment for 24 and 48 h, parasites were incubated with 200 nM Mitotracker Red CMXRos (Invitrogen) for an additional 30 min. BSF trypanosomes were washed in cold PBS and fixed with 3% PFA in PBS at 4 °C for 1 h. Fixed parasites were washed with PBS, stained with 10 μg/mL DAPI, and mounted in VECTASHIELD mounting medium (Vector Laboratories, Burlingame, CA, USA). Images were analyzed with a Nikon Eclipse 90i fluorescence microscope (Nikon, Tokyo, Japan) and captured with a digital camera (DS-1QM, Nikon).

In Vivo Experiments. BALB/C mice were infected with *T. brucei brucei* Lister 427 (3×10^4 cells) by i.p. injection. Mice were divided into groups ($n = 5$), and drug treatment was carried out for 4 consecutive days by administering compound **8** i.p. at 10, 3, 1, or 0.3 mg/kg. Parasitemia and survival were evaluated daily for 25 days. Mice showing impaired health status and/or with a parasite load $>10^8$ cells/mL of blood were euthanized.

Analysis of Mitochondrial Membrane Potential. The mitochondrial membrane potential in situ was analyzed spectrofluorometrically using safranine as the probe.[23,24] *T. brucei* PCF and BSF trypanosomes were incubated at 28 °C in reaction buffer (125 mM sucrose, 65 mM KCl, 10 mM HEPES-KOH buffer, pH 7.2, 1 mM $MgCl_2$, 2.5 mM potassium phosphate) with additions as described in the figure legends. Fluorescence changes were monitored on a Hitachi 4500 spectrofluorometer with excitation at 496 nm and emission at 586 nm.

Computational Aspects. All of the mathematical modeling was performed in R (http://www.R-project.org). Descriptors were calculated using Molecular Operating Environment (MOE).[17]

Statistical Analyses. All of the $IC_{50}/EC_{50}/CC_{50}$ values were measured in duplicate. Dose−response curves were fitted by using a sigmoidal dose−response equation with a variable slope using GraphPad Prism 6 Software (GraphPad Software, San Diego, CA, USA).

■ ASSOCIATED CONTENT

Supporting Information

The Supporting Information is available free of charge on the ACS Publications website at DOI: 10.1021/acsinfecdis.5b00068.

An additional figure illustrating the uncoupling effect of **8** (PDF)

■ AUTHOR INFORMATION

Corresponding Authors

*E-mail: eoldfiel@illinois.edu (E.O.).
*E-mail: joohwan.no@ip-korea.org (J.H.N.).

Author Contributions

#G.Y. and W.Z. contributed equally to this work.

Author Contributions

G.Y., W.Z., R.D., E.O., and J.H.N. designed the research; Y.W. and K.L. synthesized compounds; G.Y., S.Y.B., and G.C. performed cell growth inhibition assays and in vivo experiments; W.Z. and Z.H. performed enzyme inhibition assays; W.Z. performed DSC experiments and computational modeling; G.H. and S.Y.B. performed membrane potential measurements; G.Y., W.Z., R.D., E.O., and J.H.N. analyzed the data; E.O. and W.Z. wrote the paper.

Notes

The authors declare no competing financial interest.

■ ACKNOWLEDGMENTS

This work was supported by the United States Public Health Service (National Institutes of Health Grants GM065307, CA158191, and AI104120); a Harriet A. Harlin Professorship;

DOI: 10.1021/acsinfecdis.5b00068
ACS Infect. Dis. 2015, 1, 388−398

the University of Illinois/Oldfield Research Fund; and the National Research Foundation of Korea (NRF-2014K1A4A7A01074645), a grant funded by the Korean Government (MSIP), Gyeonggi-do, and KISTI. We thank David W. Boykin, Georgia State University, for the gift of DB75.

■ ABBREVIATIONS

FPPS, farnesyl diphosphate synthase; UPPS, undecaprenyl diphosphate synthase; BSF, bloodstream form; PCF, procyclic form; HEK, human embryonic kidney; human Hep, hepatocellular carcinoma; *Tb*, *Trypanosoma brucei*; SI, selectivity index; IC_{50}, half-maximal inhibitory concentration; EC_{50}, half-maximal effective concentration; CC_{50}, half-maximal cytotoxic concentration; FCCP, carbonyl cyanide 4-(trifluoromethoxy)-phenylhydrazone; MESG, 7-methyl-6-thioguanosine; GPP, geranyl diphosphate; IPP, isopentenyl diphosphate; FPP, farnesyl diphosphate

■ REFERENCES

(1) Centers for Disease Control and Prevention (Atlanta, GA). About Parasites. http://www.cdc.gov/parasites/about.html (accessed May 29, 2015).
(2) Baker, N., de Koning, H. P., Maser, P., and Horn, D. (2013) Drug resistance in African trypanosomiasis: the melarsoprol and pentamidine story. *Trends Parasitol. 29*, 110−118.
(3) Torreele, E., Bourdin Trunz, B., Tweats, D., Kaiser, M., Brun, R., Mazue, G., Bray, M. A., and Pecoul, B. (2010) Fexinidazole–a new oral nitroimidazole drug candidate entering clinical development for the treatment of sleeping sickness. *PLoS Neglected Trop. Dis. 4*, e923.
(4) Nare, B., Wring, S., Bacchi, C., Beaudet, B., Bowling, T., Brun, R., Chen, D., Ding, C., Freund, Y., Gaukel, E., Hussain, A., Jarnagin, K., Jenks, M., Kaiser, M., Mercer, L., Mejia, E., Noe, A., Orr, M., Parham, R., Plattner, J., Randolph, R., Rattendi, D., Rewerts, C., Sligar, J., Yarlett, N., Don, R., and Jacobs, R. (2010) Discovery of novel orally bioavailable oxaborole 6-carboxamides that demonstrate cure in a murine model of late-stage central nervous system African trypanosomiasis. *Antimicrob. Agents Chemother. 54*, 4379−4388.
(5) Mathis, A. M., Holman, J. L., Sturk, L. M., Ismail, M. A., Boykin, D. W., Tidwell, R. R., and Hall, J. E. (2006) Accumulation and intracellular distribution of antitrypanosomal diamidine compounds DB75 and DB820 in African trypanosomes. *Antimicrob. Agents Chemother. 50*, 2185−2191.
(6) Lanteri, C. A., Trumpower, B. L., Tidwell, R. R., and Meshnick, S. R. (2004) DB75, a novel trypanocidal agent, disrupts mitochondrial function in *Saccharomyces cerevisiae*. *Antimicrob. Agents Chemother. 48*, 3968−3974.
(7) Zhu, W., Zhang, Y., Sinko, W., Hensler, M. E., Olson, J., Molohon, K. J., Lindert, S., Cao, R., Li, K., Wang, K., Wang, Y., Liu, Y. L., Sankovsky, A., de Oliveira, C. A., Mitchell, D. A., Nizet, V., McCammon, J. A., and Oldfield, E. (2013) Antibacterial drug leads targeting isoprenoid biosynthesis. *Proc. Natl. Acad. Sci. U. S. A. 110*, 123−128.
(8) Lindert, S., Zhu, W., Liu, Y. L., Pang, R., Oldfield, E., and McCammon, J. A. (2013) Farnesyl diphosphate synthase inhibitors from *in silico* screening. *Chem. Biol. Drug Des. 81*, 742−748.
(9) Liu, Y. L., Cao, R., Wang, Y., and Oldfield, E. (2015) Farnesyl diphosphate synthase inhibitors with unique ligand-binding geometries. *ACS Med. Chem. Lett. 6*, 349.
(10) Zhu, W., Wang, Y., Li, K., Gao, J., Huang, C. H., Chen, C. C., Ko, T. P., Zhang, Y., Guo, R. T., and Oldfield, E. (2015) Antibacterial drug leads: DNA and enzyme multitargeting. *J. Med. Chem. 58*, 1215.
(11) Li, K., Schurig-Briccio, L. A., Feng, X. X., Upadhyay, A., Pujari, V., Lechartier, B., Fontes, F. L., Yang, H. L., Rao, G. D., Zhu, W., Gulati, A., No, J. H., Cintra, G., Bogue, S., Liu, Y. L., Molohon, K., Orlean, P., Mitchell, D. A., Freitas-Junior, L., Ren, F. F., Sun, H., Jiang, T., Li, Y. J., Guo, R. T., Cole, S. T., Gennis, R. B., Crick, D. C., and Oldfield, E. (2014) Multitarget drug discovery for tuberculosis and other infectious diseases. *J. Med. Chem. 57*, 3126−3139.
(12) Jacobs, R. T., Nare, B., and Phillips, M. A. (2011) State of the art in African trypanosome drug discovery. *Curr. Top. Med. Chem. 11*, 1255−1274.
(13) Opperman, T. J.; Houseweart, C.; Williams, J. D.; Peet, N. P.; Moir, D. T.; Bowlin, T. L. The Mechanism of Antibacterial Action of Novel Bis-Indole Antibiotics. Presented at the 50th Interscience Conference on Antimicrobial Agents and Chemotherapy, Boston, 2010; Paper F1-1631.
(14) Salic, A., and Mitchison, T. J. (2008) A chemical method for fast and sensitive detection of DNA synthesis in vivo. *Proc. Natl. Acad. Sci. U. S. A. 105*, 2415−2420.
(15) Zeng, C., Pan, F., Jones, L. A., Lim, M. M., Griffin, E. A., Sheline, Y. I., Mintun, M. A., Holtzman, D. M., and Mach, R. H. (2010) Evaluation of 5-ethynyl-2′-deoxyuridine staining as a sensitive and reliable method for studying cell proliferation in the adult nervous system. *Brain Res. 1319*, 21−32.
(16) da Silva, M. S., Monteiro, J. P., Nunes, V. S., Vasconcelos, E. J., Perez, A. M., Freitas-Junior, L. d. H., Elias, M. C., and Cano, M. I. (2013) *Leishmania amazonensis* promastigotes present two distinct modes of nucleus and kinetoplast segregation during cell cycle. *PLoS One 8*, e81397.
(17) *Molecular Operating Environment (MOE)*, version 2013.08; Chemical Computing Group: Montreal, QC, 2014.
(18) Montalvetti, A., Fernandez, A., Sanders, J. M., Ghosh, S., Van Brussel, E., Oldfield, E., and Docampo, R. (2003) Farnesyl pyrophosphate synthase is an essential enzyme in *Trypanosoma brucei* - *In vitro* RNA interference and in vivo inhibition studies. *J. Biol. Chem. 278*, 17075−17083.
(19) Mukkamala, D., No, J. H., Cass, L. M., Chang, T. K., and Oldfield, E. (2008) Bisphosphonate inhibition of a Plasmodium farnesyl diphosphate synthase and a general method for predicting cell-based activity from enzyme data. *J. Med. Chem. 51*, 7827−7833.
(20) Harrill, A. H., DeSmet, K. D., Wolf, K. K., Bridges, A. S., Eaddy, J. S., Kurtz, C. L., Hall, J. E., Paine, M. F., Tidwell, R. R., and Watkins, P. B. (2012) A mouse diversity panel approach reveals the potential for clinical kidney injury due to DB289 not predicted by classical rodent models. *Toxicol. Sci. 130*, 416−426.
(21) Moreno, S. N. J. (1996) Pentamidine is an uncoupler of oxidative phosphorylation in rat liver mitochondria. *Arch. Biochem. Biophys. 326*, 15−20.
(22) Lanteri, C. A., Tidwell, R. R., and Meshnick, S. R. (2008) The mitochondrion is a site of trypanocidal action of the aromatic diamidine DB75 in bloodstream forms of *Trypanosoma brucei*. *Antimicrob. Agents Chemother. 52*, 875−882.
(23) Vercesi, A. E., Bernardes, C. F., Hoffmann, M. E., Gadelha, F. R., and Docampo, R. (1991) Digitonin permeabilization does not affect mitochondrial-function and allows the determination of the mitochondrial-membrane potential of *Trypanosoma cruzi in situ*. *J. Biol. Chem. 266*, 14431−14434.
(24) Huang, G., Vercesi, A. E., and Docampo, R. (2013) Essential regulation of cell bioenergetics in *Trypanosoma brucei* by the mitochondrial calcium uniporter. *Nat. Commun. 4*, 2865.
(25) Li, K., Wang, Y., Yang, G., Byun, S. Y., Rao, G., Shoen, C., Yang, H., Gulati, A., Crick, D. C., Cynamon, M., Huang, G., Docampo, R., No, J. H., and Oldfield, E. (2015) Oxa-, thia-, heterocycle and carborane analogs of SQ109: bacterial and protozoal cell growth inhibitors. *ACS Infect. Dis. 1*, 215.
(26) Weinbach, E. C., and Garbus, J. (1969) Mechanism of action of reagents that uncouple oxidative phosphorylation. *Nature 221*, 1016−1018.
(27) Tao, H., Zhang, Y., Zeng, X., Shulman, G. I., and Jin, S. (2014) Niclosamide ethanolamine-induced mild mitochondrial uncoupling improves diabetic symptoms in mice. *Nat. Med. 20*, 1263−1269.
(28) Crunkhorn, S. (2014) Metabolic disease: Mitochondrial uncoupler reverses diabetes. *Nat. Rev. Drug Discovery 13*, 885.
(29) Oldfield, E., and Feng, X. (2014) Resistance-resistant antibiotics. *Trends Pharmacol. Sci. 35*, 664−674.

DOI: 10.1021/acsinfecdis.5b00068
ACS Infect. Dis. 2015, 1, 388−398

(30) Liu, Y. L., Lindert, S., Zhu, W., Wang, K., McCammon, J. A., and Oldfield, E. (2014) Taxodione and arenarone inhibit farnesyl diphosphate synthase by binding to the isopentenyl diphosphate site. *Proc. Natl. Acad. Sci. U. S. A. 111*, E2530−E2539.
(31) Webb, M. R. (1992) A continuous spectrophotometric assay for inorganic phosphate and for measuring phosphate release kinetics in biological systems. *Proc. Natl. Acad. Sci. U. S. A. 89*, 4884−4887.

DOI: 10.1021/acsinfecdis.5b00068
ACS Infect. Dis. 2015, 1, 388−398